OPEN ACCESS



Reionization in the Light of Dark Stars

Paolo Gondolo ^{1,2,3}, Pearl Sandick ¹, Barmak Shams Es Haghi ¹, and Eli Visbal ⁴ ⁶

Department of Physics and Astronomy, University of Utah, Salt Lake City, UT 84112, USA; shams@physics.utah.edu

Department of Physics, Tokyo Institute of Technology, Tokyo 152-8551, Japan

Kavli Institute for the Physics and Mathematics of the Universe, The University of Tokyo, Kashiwa, Chiba 277-8583, Japan

Department of Physics and Astronomy and Ritter Astrophysical Research Center, University of Toledo, Toledo, OH 43606, USA

Received 2022 February 28; revised 2022 July 8; accepted 2022 July 8; published 2022 August 9

Abstract

We investigate the effect of dark stars (DSs) on the reionization history of the universe, and the interplay between them and feedback due to Lyman–Werner (LW) radiation in reducing the cosmic microwave background (CMB) optical depth to a value within the $\tau = 0.054 \pm 0.007$ range measured by Planck. We use a semianalytic approach to evaluate reionization histories and CMB optical depths, which includes Population II stars in atomic cooling halos and Population III stars in minihalos with LW feedback, preceded by a DS phase. We show that while LW feedback by itself can reduce the integrated optical depth to the last scattering surface to ~ 0.05 only if the Population III star formation efficiency is less than $\sim 0.2\%$, the inclusion of a population of DSs can naturally lead to the measured CMB optical depth for much larger Population III star formation efficiencies $\gtrsim 1\%$.

Unified Astronomy Thesaurus concepts: Population III stars (1285); Reionisation (1383)

1. Introduction

After the recombination of electrons and protons in the universe into neutral hydrogen at redshift $z \sim 1100$, thermal photons decouple and propagate from the surface of last scattering to form the cosmic microwave background (CMB). The CMB redshifts uninterruptedly until the first ionizing sources, which are generally considered to be the first stars, form within galaxies at redshifts $z \lesssim 30$ (Gnedin 2000; Ciardi et al. 2000; Bromm et al. 2001; Schaerer 2002; Tumlinson et al. 2003; Wyithe & Loeb 2003; Benson et al. 2006). Scattering of the CMB by the reionized intergalactic medium results in an integrated optical depth τ . Explanations of the Planck measured value $\tau = 0.054 \pm 0.007$ (68% confidence level (CL); Planck Collaboration et al. 2020) with standard metal-free Population III stars struggle with overproduction of ionizing radiation for high star formation efficiencies. In this study we show that the measured optical depth can be naturally achieved by replacing some or all of the first Population III stars with dark stars (DSs), which are powered by dark matter (DM) annihilation instead of nuclear fusion (Spolyar et al. 2008). In contrast to more standard Population III stars, DSs produce a negligible amount of ionizing radiation, and typically form Population III stars at the end of their lives.

Though the nature of the first stars is, as yet, unknown, any hard ionizing radiation produced by them would have reionized the neutral gas in the intergalactic medium (IGM), a process which is completed by redshift $z\!\sim\!7$ (Fan et al. 2006; Dawson et al. 2007); afterwards the IGM remains ionized until today. The scattering of CMB photons off the resultant free electrons from reionization modifies the anisotropy power spectrum of the CMB observed today. This information is encoded in the integrated optical depth to the surface of last scattering, τ .

Population III stars presumably form from metal-free gas consisting of primordial hydrogen and helium synthesized in the early universe. Population II star formation is thought to

Original content from this work may be used under the terms of the Creative Commons Attribution 4.0 licence. Any further distribution of this work must maintain attribution to the author(s) and the title of the work, journal citation and DOI.

take place in DM minihalos with masses of $\sim 10^6 M_{\odot}$ (Haiman et al. 1996; Tegmark et al. 1997; Abel et al. 2002; Bromm et al. 2002). Formation of Population III stars in minihalos demands efficient molecular cooling, because primordial gas does not have the cooling pathways due to transitions atomic/molecular energy levels provided by metals. The cooling process can even become less efficient since formation of Population III stars is accompanied by emission of Lyman-Werner (LW) photons with energy in the 11.2-13.6 eV range, which can dissociate molecular hydrogen (Haiman et al. 1997; Machacek et al. 2001; Wise & Abel 2007; O'Shea & Norman 2008; Wolcott-Green et al. 2011; Visbal et al. 2014). Because of the photodissociation of molecular hydrogen, eventually only halos with virial temperatures $T_{\rm vir} \gtrsim 10^4 \, {\rm K}$ (atomic cooling halos) can form stars by atomic hydrogen cooling. Formation of Population III stars continues in these halos until they become metal-rich at the onset of Population I/II star formation. Population III are thought to be able to contribute significantly to reionization in that they have been shown to be more efficient at producing ionizing radiation than metalenriched stars, i.e., Population I/II stars (Tumlinson & Shull 2000: Schaerer 2002, 2003).

The small value of the CMB electron scattering optical depth measured by Planck, $\tau = 0.054 \pm 0.007$ (68% CL; Planck Collaboration et al. 2020), which is consistent with the decreasing trend of the previous measurements by Planck (Planck Collaboration et al. 2016) and WMAP (Komatsu et al. 2011), makes early reionization even more challenging than before. A novel idea to delay early star formation and reduce early partial reionization, first put forward in Scott et al. (2011), is to consider the affect of annihilation of DM particles, such as weakly interacting massive particles (WIMPs), into standard model particles at the center of minihalos, as in Spolyar et al. (2008) and subsequent works. During star formation, baryons steepen the gravitational potential within the minihalo after cooling and contracting, which draws more DM into its center. This leads to a spike in the DM annihilation rate, followed by injection of a significant amount of energy into the collapsing baryon cloud, which halts or delays star formation. DM annihilation at the core of minihalos results in a DS, a partially collapsed and cool object (Spolyar et al. 2008; Natarajan et al. 2009). For a review of DS formation, we refer to Freese et al. (2016) and references therein.

In this study, we present a new calculation of the effect of DSs on the ionization history and the corresponding integrated optical depth to the last scattering surface. The effect of the LW background on reducing the CMB optical depth by increasing the minimum critical halo mass required for cooling, which has been investigated in detail in Visbal et al. (2015), is also considered here. For a more detailed study of reionization history and the CMB polarization anisotropy in the presence of LW background, which also includes a wider range of prescriptions for modeling star formation, we refer to Ahn & Shapiro (2021). By exploring the interplay between DSs and LW feedback, we show that while LW feedback can barely reduce the CMB optical depth to meet the constraints set by Planck data for Population III star formation efficiency less than $\sim 10^{-4}$, DSs can easily decrease the CMB optical depth to satisfy the data even for Population III star formation efficiency as high as $\sim 10^{-2}$.

The outline of this paper is as follows. In Section 2, we describe our reionization model, which includes LW feedback and a description of the relevant model parameters and their fiducial values. In Section 3, after a brief review of DSs and their impact on the reionization history, we modify the reionization model to incorporate them. Finally, in Section 4 we present and discuss our results, including the effects of DSs on reionization and, consequently, on the integrated optical depth to the last scattering surface, as well as the sensitivity of the optical depth to astrophysical parameters. In this study, a Λ CDM cosmology with following values of the cosmological parameters is assumed: $\Omega_{\rm m}h^2=0.14,~\Omega_{\rm b}h^2=0.022,~h=0.67,~\sigma_8=0.81,~{\rm and}~n_{\rm s}=0.96$ (Planck Collaboration et al. 2020).

2. Reionization Model

In this section we review the semianalytic reionization model presented in Visbal et al. (2015) with LW feedback but in the absence of DSs. The inclusion of DSs is described in Section 3. The total ionized filling factor, Q(z), is given by

$$Q(z) = \rho_{\rm b}(z) \int_{\infty}^{z} dz' \left[\epsilon_{\rm a} \frac{dF_{\rm coll,i}}{dz} (z') + (1 - Q(z')) \right] \times \left(\epsilon_{\rm a} \frac{dF_{\rm coll,a}}{dz} (z') + \epsilon_{\rm m} \frac{dF_{\rm coll,m}}{dz} (z') \right) V(z', z), \quad (1)$$

where $\rho_b(z)$ is the mean cosmic baryon density, V is the volume of the ionized region, $\epsilon_{\{m,a\}}$ represent the ionizing efficiency, and $F_{\text{coll},\{m,a,i\}}$ are the total fraction of the mass in the universe collapsed into DM halos at redshift z', where the subscripts m, a, and i indicate molecular hydrogen cooling halos, atomic hydrogen cooling halos, and halos above the ionized IGM cutoff. In this model, it is assumed that all molecular hydrogen cooling halos host Population III stars and all atomic hydrogen cooling halos host Population II stars. Specifically, $\epsilon_a = f_{*,a} f_{esc,a} \eta_{ion,a}$ is the ionizing efficiency of atomic cooling halos hosting Population II stars, and $\epsilon_{\rm m} = f_{*,{\rm m}} f_{\rm esc,m} \eta_{\rm ion,m}$ is the ionizing efficiency in minihalos that host Population III stars. These factors $\epsilon_{\{m,a\}}$ count the number of ionizing photons escaping into the IGM per baryon contained in a DM halo and depend on the star formation efficiency (the fraction of baryons in minihalos that form stars), $f_{*,m}$, the ionizing photon escape fraction, $f_{\rm esc,m}$, and the number of

ionizing photons produced per baryon included in stars, $\eta_{\text{ion,m}}$. The fiducial values of these parameters are taken as follows: $f_{*,m} = 0.001, \quad f_{esc,m} = 0.5,$ $\eta_{\text{ion,m}} = 80,000,$ $\eta_{\text{ion,a}} = 4000$, and $f_{*,a} = f_{*,a}(z)$ is assumed to be the "redshiftdependent" star formation efficiency case in Visbal et al. (2015). The ionizing photons produced per baryon in Population II and Population III stars ($\eta_{\text{ion,m}}$ and $\eta_{\text{ion,a}}$, respectively) are well understood from stellar evolution modeling (Schaerer 2002; Samui et al. 2007). The Population II star formation efficiency, $f_{*,a}(z)$, is calibrated via abundance matching of DM halos and the observed UV luminosity function at $z \approx 6$ (see Visbal et al. 2015, for details). We note that there is significant uncertainty in this quantity since the star formation efficiency must be extrapolated to higher redshifts and smaller galaxies than are actually observed. Our choice of Population III star formation efficiency, $f_{*,m}$, corresponds to a $\sim 100\,M_{\odot}$ of Population III stars in a $\sim 10^6\,M_{\odot}$ minihalo. While we believe this is a reasonable choice, we note that this crucial parameter has significant uncertainty. For example, the hydrodynamical cosmological simulations of Skinner & Wise (2020) find most minihalos with efficiencies between 10^{-3} and 10^{-4} , while a much higher value (0.38) has been found to be consistent with a variety of observables in a recent semianalytic study (Hartwig et al. 2022). The escape fractions are generally consistent with the hydrodynamical radiative transfer simulations of Wise et al. (2014), but should also be regarded as uncertain. Overall, we emphasize that we have chosen a reasonable set of fiducial parameters guided by numerical simulations and observational constraints. However, due to the lack of direct observations of the first stars and galaxies there are necessarily significant uncertainties. Our findings discussed below motivate additional theoretical and observational work to more tightly constrain the star formation efficiencies and escape fractions for low-mass high-redshift DM halos.

In this model, the number of DM halos per unit comoving volume of the universe is evaluated analytically with the Sheth–Tormen mass function (Sheth & Tormen 1999). In the regions of the IGM that have already been ionized, star formation below a halo mass scale, $M_{\rm i}(z)=1.5\times 10^8 \left(\frac{1+z}{11}\right)^{-1.5} M_{\odot}$ (Dijkstra et al. 2004), is prevented by the increased Jeans mass of the heated gas. The masses of atomic cooling halos that host Population II stars are assumed to be larger than $M_{\rm a}(z)=5.4\times 10^7 \left(\frac{1+z}{11}\right)^{-1.5} M_{\odot}$ (Fernandez et al. 2014). The minimum mass of minihalos hosting Population III stars, which is sensitive to the LW background (flux), $J_{\rm LW}(z)$, and the baryon–DM streaming velocity, $v_{\rm bc}$, will be discussed later.

The total fraction of the mass in the universe that is collapsed into DM halos above the ionized IGM cutoff, $F_{\rm coll,i}(z)$, atomic cooling halos, $F_{\rm coll,a}(z)$, and minihalos, $F_{\rm coll,m}(z)$, are given by

$$F_{\text{coll,i}}(z) = \frac{1}{\Omega_{\text{m}}\rho_{\text{c}}} \int_{M_{\text{i}}}^{\infty} dMM \frac{dn}{dM}(z),$$

$$F_{\text{coll,a}}(z) = \frac{1}{\Omega_{\text{m}}\rho_{\text{c}}} \int_{M_{\text{a}}}^{M_{\text{i}}} dMM \frac{dn}{dM}(z),$$

$$F_{\text{coll,m}}(z) = \frac{1}{\Omega_{\text{m}}\rho_{\text{c}}} \int_{M_{\text{m}}}^{M_{\text{a}}} dMM \frac{dn}{dM}(z),$$
(2)

respectively, where ρ_c is the critical energy density and dn(z)/dM is the Sheth-Tormen mass function.

The factor 1-Q(z) is included to make sure that new ionizing sources appear in minihalos and atomic cooling halos only in regions that have not yet been ionized (Haiman & Holder 2003). V(z',z) represents the expanding ionized region into the IGM where the corresponding halo has formed at z' ($z \le z'$). The evolution of the ionization front, $R_i = [3V/(4\pi)]^{1/3}$, is governed by

$$\frac{dR_{\rm i}^3}{dt} = 3H(z)R_{\rm i}^3 + \frac{3\dot{N}_{\gamma}}{4\pi\langle n_H \rangle} - C(z)\langle n_H \rangle \alpha_{\rm B}R_{\rm i}^3, \tag{3}$$

where H(z) is the Hubble expansion rate, $\langle n_H \rangle$ is the mean hydrogen density in universe, and $C(z) \equiv \langle n_{\rm H\,II}^2 \rangle / \langle n_{\rm H\,II} \rangle^2 = 2 \left(\frac{1+z}{7}\right)^{-2} + 1$ is the clumping factor of the ionized IGM (Bauer et al. 2015). $\alpha_{\rm B} = 2.6 \times 10^{-13} \, {\rm cm}^3 \, {\rm s}^{-1}$ is the case B (optically thick) recombination coefficient of hydrogen at $T = 10^4 \, {\rm K}$. The rate of ionizing photon emission, for each solar mass of star-forming gas with ionizing efficiency normalized to one, \dot{N}_{γ} , is given by

$$\dot{N}_{\gamma}(t) = \dot{N}_{0}[\theta(t_{6.5} - t) + (t/t_{6.5})^{-4.5}\theta(t - t_{6.5})],\tag{4}$$

where $\dot{N}_0 = 9.25 \times 10^{42} \, {\rm s}^{-1} \, M_\odot^{-1}$, $\theta(t)$ is the unit step function, $t_{6.5} = 10^{6.5}$ yr, and t is measured after starburst. This rate of ionizing photon emission results in one ionizing photon per baryon incorporated into stars over the lifetime of the stellar population. We note that the time dependence of Equation (4) corresponds to a starburst with a Salpeter initial mass function and a metallicity equal to 2% of the solar value (Leitherer et al. 1999; Haiman & Holder 2003). Because the production of ionized photons from a particular source is essentially instantaneous compared to the timescales on which the IGM is reionized, our results are insensitive to the precise form used in Equation (4).

The minimum mass of minihalos hosting Population III star formation, $M_{\rm m}$, is affected by LW radiation and the baryon–DM streaming velocity. Increased LW radiation leads to an increased fraction of dissociated molecular hydrogen, which increases $M_{\rm m}$. Similarly, an increased streaming velocity delays the inflow of gas into halos (Tseliakhovich & Hirata 2010), which also increases $M_{\rm m}$ (Greif et al. 2012; Stacy et al. 2012; Fialkov 2014; Schauer et al. 2019). These two effects are included in Equation (1) via $M_{\rm m}$ in Equation (2). In this study, we consider two functional forms for the dependence of $M_{\rm m}$ on redshift, both based on hydrodynamical cosmological simulations. In the first form, the effect of the baryon–DM streaming velocity is ignored, and $M_{\rm m}$ depends only on the density of LW radiation, $J_{\rm LW}$ (Fialkov et al. 2013):

$$M_{\rm m}(J_{\rm LW}, z) = 2.5 \times 10^5 \left(\frac{1+z}{26}\right)^{-1.5} \times [1 + 6.96(4\pi J_{\rm LW}(z))^{0.47}] M_{\odot}.$$
 (5)

In the second form, the baryon-DM streaming velocity $v_{\rm bc}$ is included, and the following fit formula is used for $M_{\rm m}$

(Kulkarni et al. 2021):

$$M_{\rm m}(J_{\rm LW}, \nu_{\rm bc}, z) = 1.96 \times 10^{5} (1 + J_{\rm LW}(z))^{0.8} \left(1 + \frac{\nu_{\rm bc}}{30}\right)^{1.83} \times \left(1 + \frac{J_{\rm LW}(z)\nu_{\rm bc}}{3}\right)^{-0.06} \left(\frac{1+z}{21}\right)^{\alpha(J_{\rm LW}, \nu_{\rm bc})} M_{\odot}.$$
(6)

Here

$$\alpha(J_{LW}, \nu_{bc}) = -1.64(1 + J_{LW}(z))^{0.36} \left(1 + \frac{\nu_{bc}}{30}\right)^{-0.62} \times \left(1 + \frac{J_{LW}(z)\nu_{bc}}{3}\right)^{0.13}, \tag{7}$$

 $J_{\rm LW}$ is measured in units of $10^{-21}\,{\rm erg~s^{-1}~cm^{-2}~Hz^{-1}~Sr^{-1}}$, and $\nu_{\rm bc}$ is measured in km s⁻¹. The fiducial value of the baryon–DM streaming velocity is assumed to be $30\,{\rm km\,s^{-1}}$ (Kulkarni et al. 2021). For this fit formula, simulations have been updated such that they include the effect of molecular hydrogen self-shielding, which acts to lower the minimum halo mass for Population III star formation (the opposite of the effect of the streaming velocity) (Kulkarni et al. 2021).

Provided that the IGM is almost transparent to LW photons until they are redshifted into a Lyman series line and absorbed, or equivalently by assuming that at redshift z all LW photons emitted from sources at 1.015z are observable (since an LW photon can redshift by 1.5% before reaching a Lyman series line), the intensity of the LW background can be evaluated by

$$J_{LW}(z) = \frac{c(1+z)^3}{4\pi} \int_{1.015z}^{z} dz' \frac{dt_{H}}{dz'} \left(\frac{SFRD_{a}(z')}{m_{p}} \eta_{LW,a} + \frac{SFRD_{m}(z')}{m_{p}} \eta_{LW,m} \right) E_{LW} \Delta \nu_{LW}^{-1},$$
(8)

where c is the speed of light, $t_{\rm H}$ is the Hubble time, and SFRD_{a,m}(z) are the star formation rate densities for atomic (a) and molecular (m) cooling halos, given by

$$SFRD_{a}(z) = \rho_{b} f_{*,a} \frac{dF_{coll,a}}{dt} (1 - Q(z)) + \rho_{b} f_{*,a} \frac{dF_{coll,i}}{dt},$$

$$SFRD_{m}(z) = \rho_{b} f_{*,m} \frac{dF_{coll,m}}{dt} (1 - Q(z)). \tag{9}$$

Here, $m_{\rm p}$ is the proton mass, $\eta_{\rm LW}$ counts the number of LW photons per baryon produced by stars, $E_{\rm LW}=1.9\times10^{-11}\,{\rm erg}$, and $\Delta\nu_{\rm LW}=5.8\times10^{14}\,{\rm Hz}$.

After solving Equation (1) iteratively for Q(z) and $J_{LW}(z)$, the ionized filling factor can be used to evaluate the optical depth as

$$\tau(z) = \int_0^z dz' \frac{c(1+z')^2}{H(z')} Q(z') \sigma_{\rm T} \langle n_H \rangle \left(1 + \eta_{\rm He}(z') \frac{Y}{4X} \right), \tag{10}$$

where σ_T is the Thompson scattering cross section, Y = 0.24 and X = 0.76 are the mass fractions of helium and hydrogen respectively, and $\eta_{He}(z) = \theta(z-3) + 2\theta(3-z)$, provided that

helium and hydrogen are singly ionized at the same time while helium is doubly ionized at z = 3.

3. Adding Dark Stars

The impact of DSs on the reionization history has been studied in Scott et al. (2011), which we briefly review here. The role of DM in the formation of Population III stars is not limited to providing potential wells for baryonic collapse. It has been shown that DM annihilation into standard model particles may grow drastically when baryons contract within minihalos during star formation, and may result in the formation of a new phase of stars, called DSs, powered by the annihilation of DM inside them rather than nuclear fusion (Spolyar et al. 2008). DSs have low surface temperatures and do not emit any relevant amount of ionizing radiation. Eventually, when the DM annihilation runs out, the DS phase ends with the star becoming either a Population III star or, if very massive, in direct collapse to a black hole (Spolyar et al. 2008; Natarajan et al. 2009).

There are three conditions for the formation of a DS: high DM density, trapping the DM annihilation products inside the protostar, and domination of DM heating over other heating or cooling processes (Spolyar et al. 2008). These criteria are also required throughout the evolution of the DS phase. By assuming a polytropic model for DSs and an initial mass $M \sim 1-10~M_{\odot}$ (when the DM heating becomes important), it has been shown that DSs can live $\sim 10^6$ yr by burning their DM content at formation (Freese et al. 2008), but can also live much longer and grow via accretion of baryons from the surrounding halo up to masses of $M \sim 10^7 \, M_{\odot}$ (Spolyar et al. 2009), as long as there is enough DM to fuel them. DSs have been shown to be large (e.g., tens of au), cool (surface temperature $\lesssim 10^4$ K), and very bright (luminosities $\sim 10^{11} L_{\odot}$) (Freese et al. 2008). These results have also been confirmed and improved upon by solving the stellar structure equations self-consistently, without restrictive assumptions of polytropic configurations (Rindler-Daller et al. 2015).

DSs require a dense reservoir of DM at the center of the protostar. Gravitational contraction of baryonic gas during the collapse steepens the gravitational potential in the core of the halo, which drags more DM into the center of the cloud, providing adequate DM fuel for the DS. The DM fuel can also be replenished if DM is captured into the core of stars by losing kinetic energy through scattering off nucleons in the star. The evolution and lifetime of DSs depends on the rate of DM accumulation. DM provided by gravitational contraction may run out in ~0.4 Myr, though this lifetime depends on the type of orbits experienced by the DM particles (e.g., circular or centrophilic). DM capture by DSs can also continue and keep them alive as long as they lie within a region with high enough DM density (Spolyar et al. 2009). It has been shown that for the most simplistic DS scenarios (polytropic, circular DM particle orbits, no DM capture by scattering with nuclei), the DS phase does not affect the reionization history, but reionization can be noticeably delayed if the DS lifetime is prolonged, e.g., by capture of DM via scattering off nucleons in the star (Scott et al. 2011).

For simplicity, we assume that DM annihilation contributes substantially into the energy budget of the star, and that the capture rate is sufficiently large to keep the star cool and make its contribution to reionization almost zero (Spolyar et al. 2008; Scott et al. 2011). DSs are described by two parameters of interest in this study: the DS mass fraction, f_{DS} , that describes

the fraction of the baryonic mass that initially goes into DSs rather than Population III stars, and the lifetime of DSs, t_{DS} .

To model the reionization process from star formation in DM halos, we modify the model presented in Visbal et al. (2015) to include the effect of DSs on delaying formation of Population III stars. The impact of DSs on reionization is simplified by assuming that DSs, which contain a fraction $f_{\rm DS}$ of the baryonic mass, halt reionization by delaying star formation in minihalos and atomic cooling halos during their lifetime ($t' \lesssim t \lesssim t'_{\rm DS} \equiv t' + t_{\rm DS}$) and contribute nothing to reionization, but after they run out of DM ($t \gtrsim t'_{\rm DS}$), they die and are replaced with either Population III or Population II stars. This is achieved by modifying Equation (1) to

$$Q(z) = \rho_{b}(z) \int_{\infty}^{z} dz' \left[\epsilon_{a} \frac{dF_{\text{coll,i}}}{dz} (z') + (1 - Q(z')) \right]$$

$$\times \left(\epsilon_{a} \frac{dF_{\text{coll,a}}}{dz} (z') + \epsilon_{m} \frac{dF_{\text{coll,m}}}{dz} (z') \right)$$

$$\times \phi(z', z'_{DS}, f_{DS}) [V(z', z),$$
(11)

where

$$\phi(z', z'_{DS}, f_{DS}) = (1 - f_{DS})\theta(z' - z'_{DS}) + \theta(z'_{DS} - z'),$$
(12)

and z'_{DS} is the redshift at time t'_{DS} .

4. Results

In this section, we present the results of the reionization model modified by adding DSs. In Section 4.1, we show how the total ionized filling factor and subsequently the optical depth of the fiducial reionization model change in the presence of DSs. In Section 4.2, we explore the effects of varying the astrophysical parameters on the reionization model for a benchmark DS example.

In Figure 1, we display contours of the integrated optical depth to the last scattering surface as a continuous function of $f_{\rm DS}$ and $t_{\rm DS}$. The astrophysical parameters assume their fiducial values listed at the beginning of Section 2. The top (bottom) panel corresponds to the representation of $M_{\rm m}$ in which the effect of the baryon–DM streaming velocity is ignored (included). The left (right) panels in Figure 1 show the optical depth in the presence of DSs when LW feedback is ignored (included). The red shaded regions in Figure 1 (and in the rest of the figures in this paper) display 1σ regions based on the integrated optical depth to the last scattering surface observed by Planck, i.e., $\tau = 0.054 \pm 0.007$ (Planck Collaboration et al. 2020).

From the left panels of Figure 1, we can see that the two representations of $M_{\rm m}$, in the lack of LW feedback and in the presence of DSs, lead to almost the same result. Namely, DSs with a lifetime in the range $100\,{\rm Myr} \lesssim t_{\rm DS} \lesssim 1000\,{\rm Myr}$ and with a mass fraction in the range $0.95 \lesssim f_{\rm DS} \lesssim 1$, give rise to the optical depth consistent with limits from Planck.

The right panels of Figure 1, on the other hand, indicate further suppression of the optical depth after adding the LW feedback, and also show that the effect of LW feedback is stronger for the $M_{\rm m}$ in which the baryon–DM streaming velocity is ignored, i.e., $M_{\rm m}(J_{\rm LW}, z)$, than when it includes the baryon–DM streaming velocity, i.e., $M_{\rm m}(J_{\rm LW}, \nu_{\rm bc}, z)$. After including LW feedback, for the choices $M_{\rm m}(J_{\rm LW}, z)$ and $M_{\rm m}(J_{\rm LW}, \nu_{\rm bc}, z)$, respectively, DSs with a lifetime in the range 100 Myr $\lesssim t_{\rm DS} \lesssim 1000$ Myr and with a

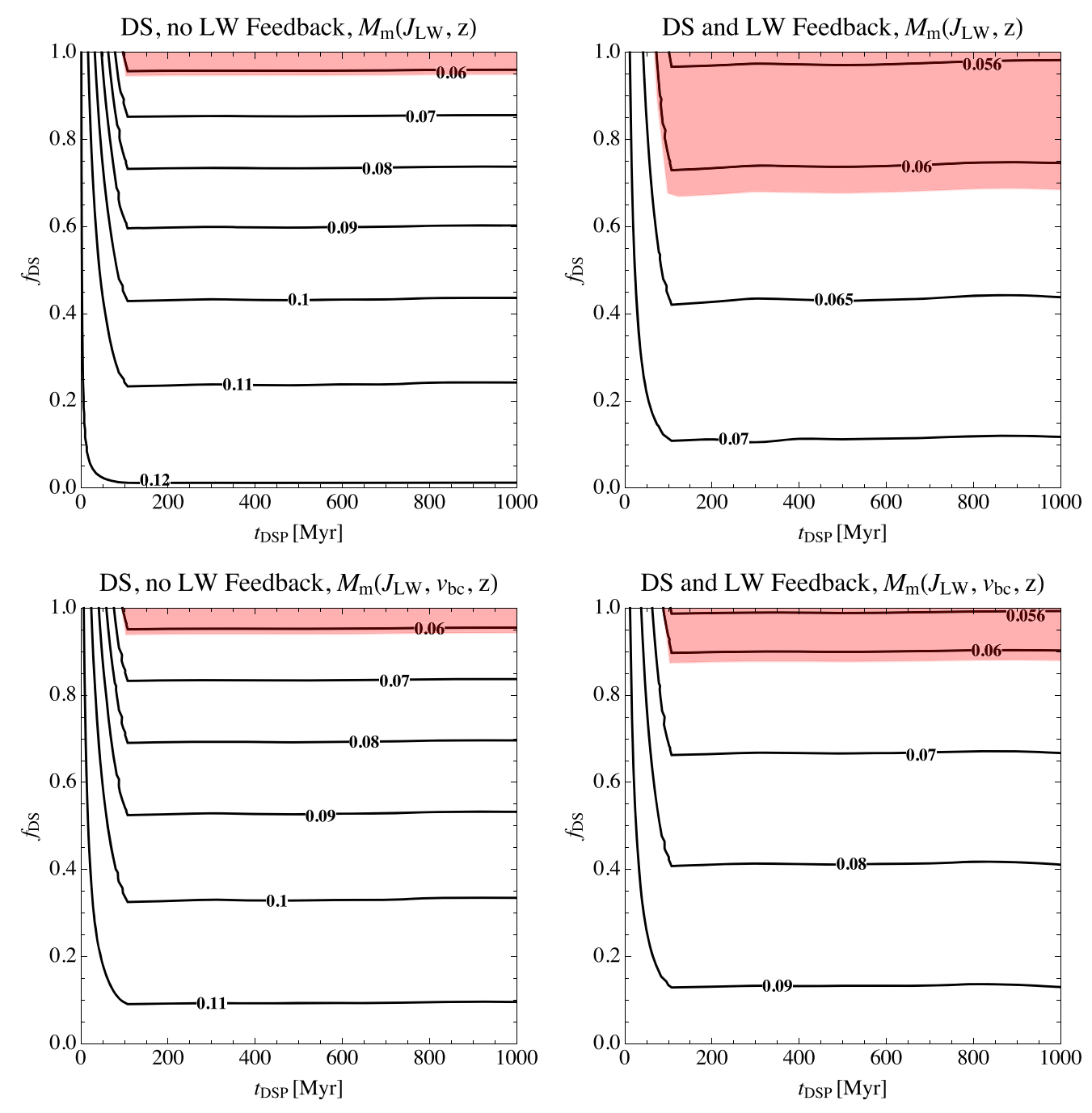


Figure 1. Contours of the integrated optical depth to the last scattering surface as a function of DSs mass fraction, f_{DS} , and the lifetime of DSs, t_{DS} . Top (bottom) panel corresponds to the minimum mass of minihalos, $M_{\rm m}$, in which the effect of the baryon–DM streaming velocity is ignored (included). Left (right) panels show the optical depth in presence of DSs when LW feedback is ignored (included). The astrophysical parameters assume their fiducial values. The red shaded regions display 1σ regions based on the integrated optical depth to the last scattering surface observed by Planck ($\tau = 0.054 \pm 0.007$) (Planck Collaboration et al. 2020).

mass fraction in the range $0.7 \lesssim f_{\rm DS} \lesssim 1$ ($0.9 \lesssim f_{\rm DS} \lesssim 1$, respectively) lead to an optical depth consistent with limits from Planck. It is worth mentioning that small values of $f_{\rm DS}$ do not produce a small enough integrated optical depth to the last scattering surface consistent with Planck measurement. This conclusion is in agreement with previous studies, e.g., Scott et al. (2011).

To elaborate on these results, in Figure 2 we display the total ionized filling factor (left panels) and corresponding optical depth from the present day to redshift z (right panels) for some benchmark DSs. The benchmark values of $t_{\rm DS}$ and $f_{\rm DS}$ used in Figure 2 have been chosen just to illustrate the behavior of the the total ionized filling factor when DSs can explain the Planck

optical depth. The top (bottom) panel corresponds to the representation of $M_{\rm m}$ in which the effect of the baryon–DM streaming velocity is ignored (included). DS parameters are chosen such that the resultant optical depth lies within the 1σ Planck region.

The gray solid curve corresponds to a reionization history without DSs and LW feedback. The gray dashed curve depicts the effect of LW feedback in the absence of DSs. The blue and magenta curves correspond to reionization histories that involve DSs with $t_{\rm DS} = 200$ Myr, $f_{\rm DS} = 0.95$ and $t_{\rm DS} = 900$ Myr, $f_{\rm DS} = 0.98$ respectively, without including LW feedback. The brown curve shows the total ionized filling factor for DSs with

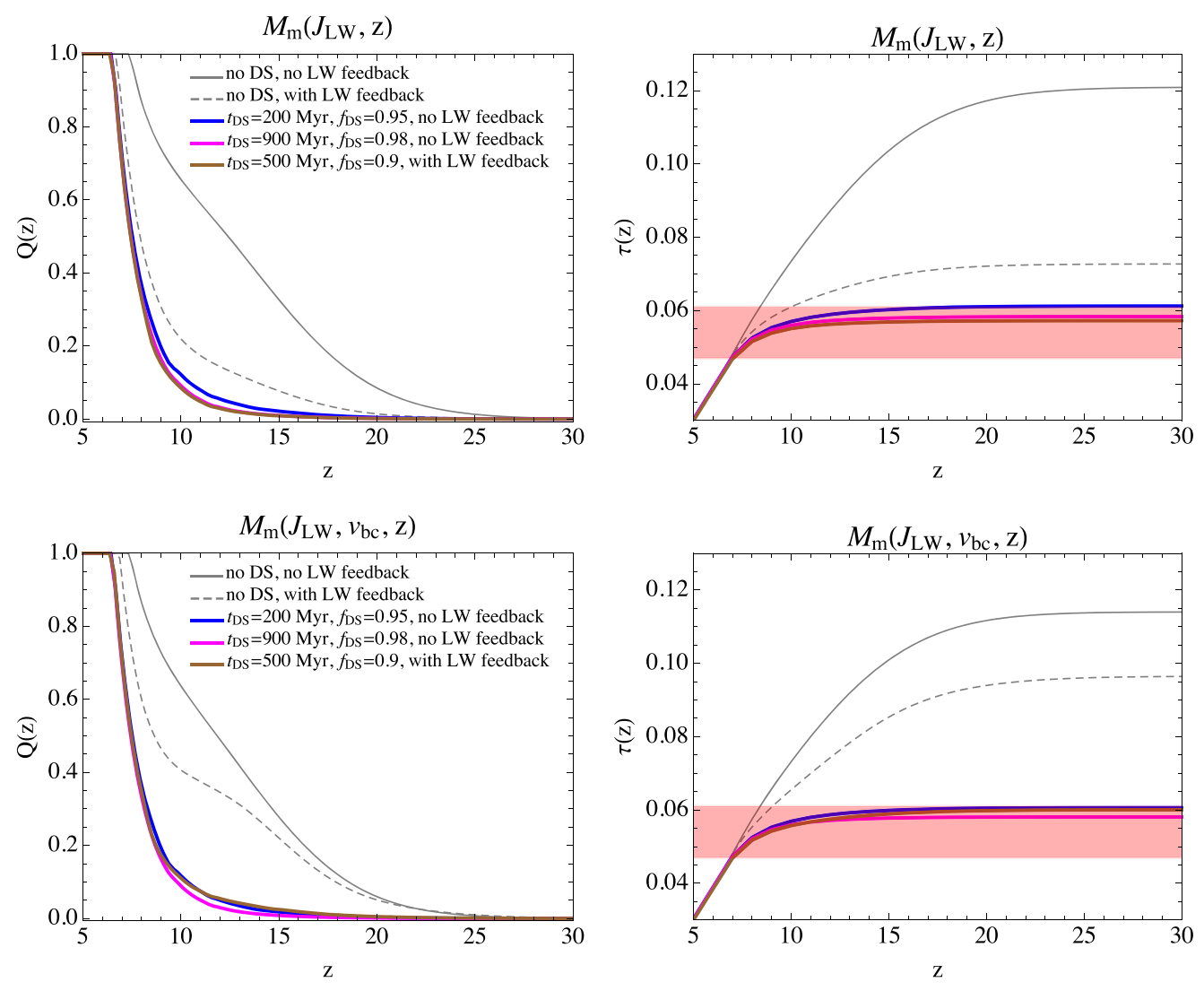


Figure 2. The total ionized filling factor (left panels) and corresponding optical depth from the present day to redshift z (right panels). Top (bottom) panel corresponds to the representation of $M_{\rm m}$ in which the effect of the baryon–DM streaming velocity is ignored (included). Gray solid (dashed) curves correspond to a reionization history without DSs and in the absence (presence) of LW feedback. Blue and magenta curves display reionization histories without LW feedback including DSs with $t_{\rm DS} = 200$ Myr, $f_{\rm DS} = 0.95$ and $t_{\rm DS} = 900$ Myr, $f_{\rm DS} = 0.98$ respectively. The brown curves show reionization in the presence of DSs with $t_{\rm DS} = 500$ Myr, $f_{\rm DS} = 0.98$ by including LW feedback. The red bands in the right panels display 1σ regions based on the integrated optical depth to the last scattering surface observed by Planck.

 $t_{\rm DS} = 500 \, {\rm Myr}, f_{\rm DS} = 0.9$ in the presence of LW feedback, where these two factors together suppress the optical depth to the acceptable level. Figure 2 displays clearly the dominance of DSs over LW feedback in decreasing the optical depth.

Previous studies (e.g., Schleicher et al. 2009; Scott et al. 2011) have utilized a Press-Schechter formalism to describe the growth of ionized regions and they treated all the halos equally considering the cooling mechanism, while in this study, the more accurate Sheth-Tormen mass function is used and halos, which are divided into molecular hydrogen cooling halos, atomic hydrogen cooling halos, and halos above the ionized IGM cutoff are handled differently. More specifically, in our analysis, the factor 1 - Q(z') in Equation (1) takes into account the fact that new ionizing sources should appear in atomic hydrogen cooling halos and molecular hydrogen cooling halos only in regions that have not yet been ionized. These differences in ionization model leads to slightly different total ionized filling factors. Regarding DSs, in Scott et al. (2011), ionization models are considered that are more involved and accurate than the one used in this study. For

example, the allowed lifetimes of the different DS phases is treated carefully and the small contribution of DSs to reionization is not neglected. These differences also lead to somewhat different total ionized filling factors. In spite of using a different ionization model and also a less sophisticated analysis, our result for the integrated optical depth without including LW feedback is in good agreement with those of Schleicher et al. (2009) and Scott et al. (2011): DSs by themselves can explain the small value of the measured integrated optical depth as long as they acquire a large mass fraction (close to 1).

4.2. Effects of Astrophysical Parameters

In Figure 3, we show contours of the integrated optical depth to the last scattering surface as a continuous function of $f_{*,\rm m}$ and $\epsilon_{\rm a}$, for $M_{\rm m}=M_{\rm m}(J_{\rm LW},z).$ Dependence on $\epsilon_{\rm a}$ is represented by the ratio, $\epsilon_{\rm a}/\epsilon_{\rm a,0}$, which captures the reduction compared to the fiducial value $\epsilon_{\rm a,0}.$ The left (right) panel displays the result in the absence of DSs and without (with) LW feedback. For $f_{*,\rm m}\lesssim 2\times 10^{-4},$ by selecting a small enough $\epsilon_{\rm a},$ the resultant

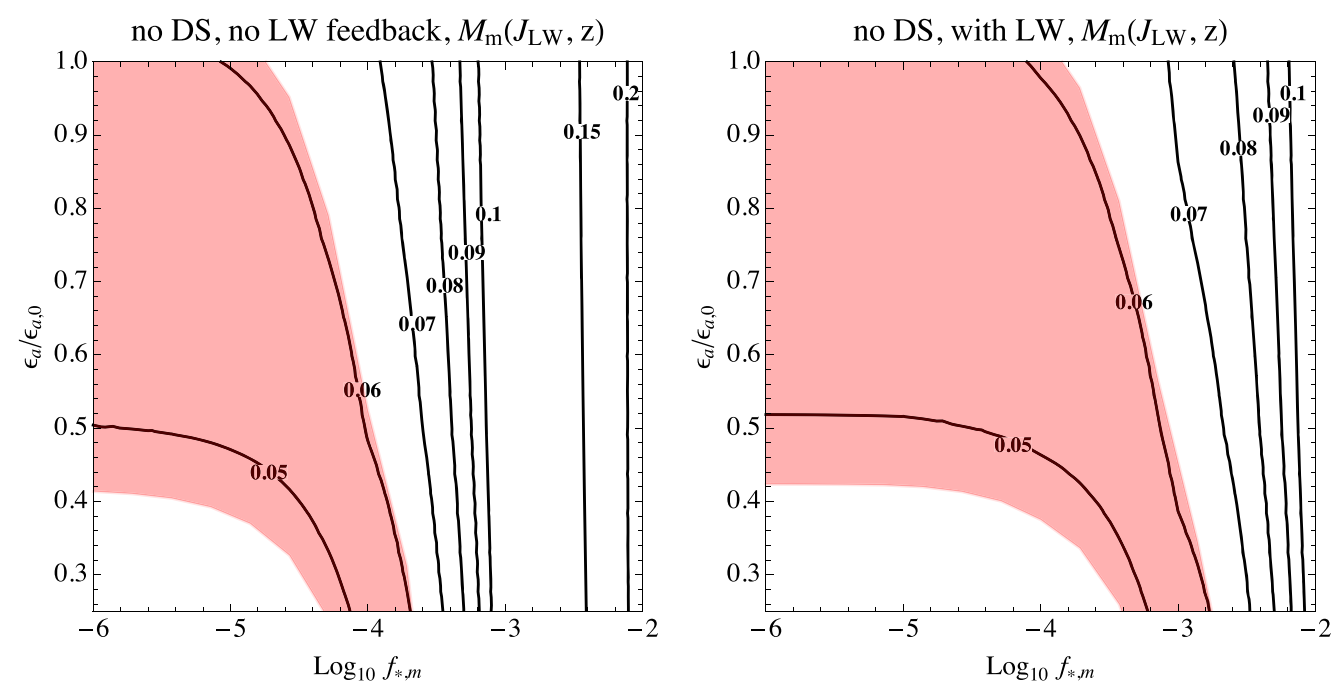


Figure 3. Contours of the integrated optical depth to the last scattering surface as a function of $f_{*,m}$ and ϵ_a , when $M_m = M_m (J_{LW}, z)$. Left (right) panel shows the optical depth without DSs when LW feedback is ignored (included). The red shaded regions display 1σ regions based on the integrated optical depth to the last scattering surface observed by Planck.

integrated optical depth could be consistent with Planck data without DSs or LW feedback. Including LW feedback makes it possible to increase the value of $f_{*,m}$ up to 2×10^{-3} . It can also be concluded from Figure 3 that for small values of $f_{*,m}$, the optical depth depends on both $f_{*,m}$ and ϵ_a , while larger values of $f_{*,m}$ dominate over ϵ_a such that the integrated optical depth is almost independent of ϵ_a .

In Figure 4 we present contours of the integrated optical depth to the last scattering surface in the $(f_{*,\rm m},\,\epsilon_{\rm a}/\epsilon_{\rm a,0})$ plane in the presence of DSs with $t_{\rm DS}=500\,{\rm Myr},\,f_{\rm DS}=0.95$. The top (bottom) panel of Figure 4 corresponds to $M_{\rm m}=M_{\rm m}(J_{\rm LW},\,z)$ ($M_{\rm m}=M_{\rm m}(J_{\rm LW},\,\nu_{\rm bc},\,z)$). The left (right) panel of Figure 4 shows contours of the integrated optical depth to the last scattering surface without (by) including LW feedback.

As Figures 3 and 4 show clearly, while LW feedback by itself can only decrease the integrated optical depth down to $\tau \simeq 0.05$, which demands small values of $f_{*,m}$ and ϵ_a , DSs can explain the small value of the measured integrated optical depth for larger values of $f_{*,m}$ and ϵ_a . This also is shown in Figure 5, which depicts the integrated optical depth to the last scattering surface as a function of $f_{*,m}$ when $\epsilon_a = \epsilon_{a,0}$ and for $M_m = M_m(J_{LW}, z)$.

In Figure 5, the gray solid curve displays the integrated optical depth without DSs and LW feedback; the gray dashed curve shows the effect of adding LW feedback; the purple solid (dashed) curve corresponds to DSs with $t_{\rm DS} = 500$ Myr, $f_{\rm DS} = 0.95$ without (with) LW feedback; and the orange solid (dashed) curve represents DSs with $t_{\rm DS} = 900$ Myr, $f_{\rm DS} = 1$ without (with) LW feedback. Although the impact of the LW feedback can be important for large values of $f_{*,\rm m}$ (purple solid and dashed curves), it becomes subdominant when increasing the lifetime of DSs or their mass fraction (orange solid and dashed curves).

5. Conclusions

We have studied the effect of DSs on the reionization history of the universe and the interplay between them and LW feedback in explaining the small value of the integrated optical depth to the last scattering surface measured by Planck. After modifying a semianalytical reionization model, which incorporates Population II stars in atomic cooling halos and Population III stars in minihalos with LW feedback, to include DSs as the first phase in star formation, we calculated the total ionized filling factor and, subsequently, the CMB optical depth.

To capture the effect of LW feedback on increasing the minimum mass of minihalos hosting Population III stars and consequently delaying the formation of these stars, we adopted two representations of the minimum mass of minihalos; the first representation only depends on LW radiation, while the second one depends on LW radiation and the baryon-DM streaming velocity. We showed that these two representations, in the absence of LW feedback, lead to almost the same results for the integrated optical depth in the presence of DSs: DSs with a lifetime in the range $100 \,\mathrm{Myr} \lesssim t_\mathrm{DS} \lesssim 1000 \,\mathrm{Myr}$ and with a mass fraction in the range $0.95 \lesssim f_{\rm DS} \lesssim 1$ give rise to an optical depth consistent with Planck measurements. With the inclusion of LW feedback, the minimum mass of minihalos that ignore the baryon-DM streaming velocity leads to stronger suppression of the integrated optical depth in the presence of DSs than the minimum mass of minihalos that depends on the baryon-DM streaming velocity: DSs, with a lifetime in the range $100 \,\mathrm{Myr} \lesssim t_\mathrm{DS} \lesssim 1000 \,\mathrm{Myr}$ and with a mass fraction in the range $0.7 \lesssim f_{\rm DS} \lesssim 1$ ($0.9 \lesssim f_{\rm DS} \lesssim 1$), generate the optical depth consistent with limits from Planck for $M_{\rm m}(J_{\rm LW}, z) \ (M_{\rm m}(J_{\rm LW}, v_{\rm bc}, z)).$

We also studied the effects of astrophysical parameters including the star formation efficiency in minihalos hosting Population III stars and the ionizing efficiency of atomic cooling halos hosting Population II stars. We find that for small values of $f_{*,m}$ the optical depth depends on both $f_{*,m}$ and ϵ_a , while for larger values of $f_{*,m}$ the integrated optical depth is almost independent of ϵ_a . We showed that in the absence of DSs, LW feedback can reduce the integrated optical depth to be consistent with the observed data by Planck for $f_{*,m} \lesssim 10^{-4}$ for

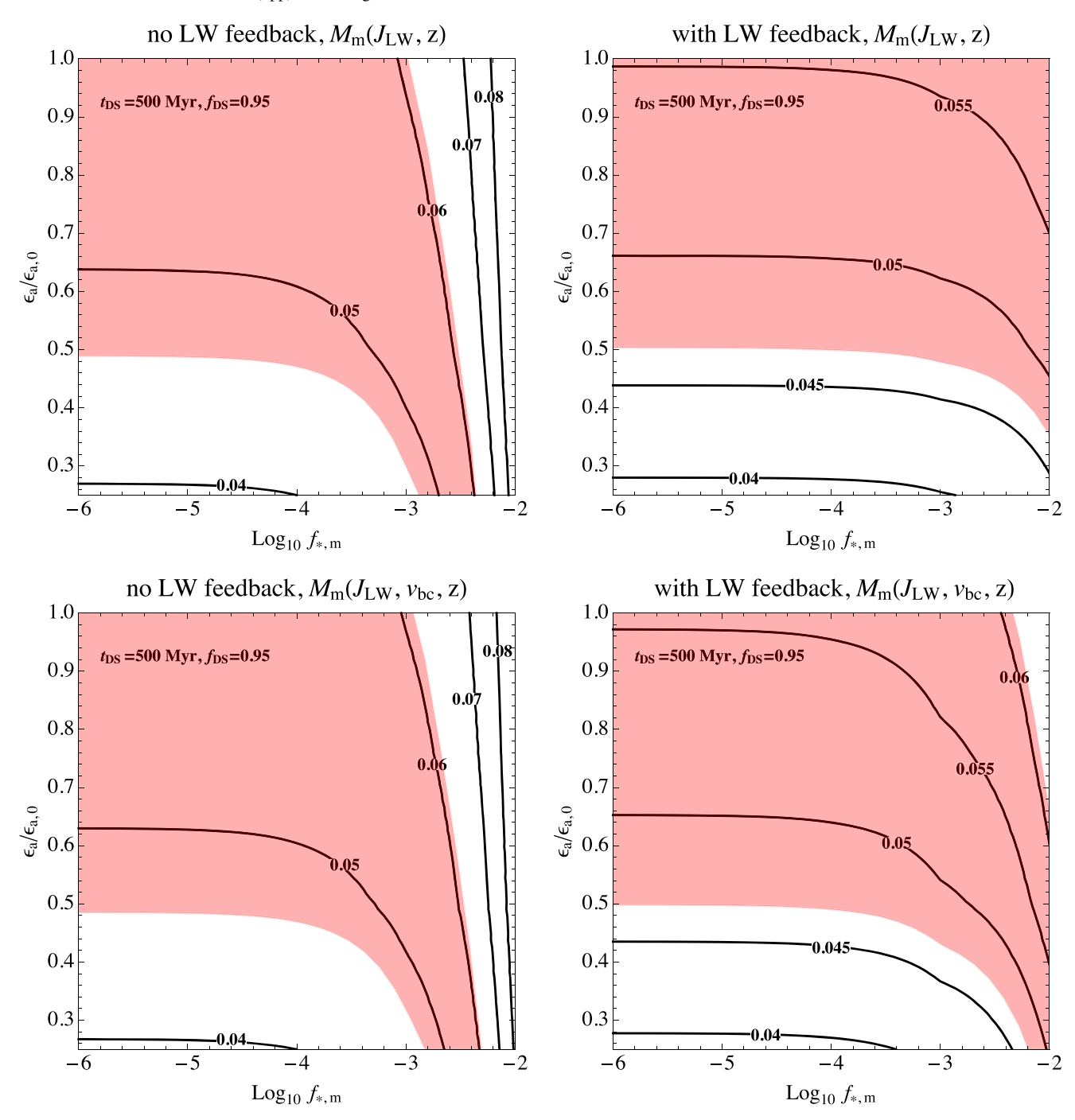


Figure 4. Contours of the integrated optical depth to the last scattering surface as a function of $f_{*,m}$ and ϵ_a in the presence of DSs with $t_{DS} = 500$ Myr, $f_{DS} = 0.95$. Top (bottom) panel corresponds to the minimum mass of minihalos, M_m , in which the effect of the baryon–DM streaming velocity is ignored (included). Left (right) panels show the optical depth when LW feedback is ignored (included). The red shaded regions display 1σ regions based on the integrated optical depth to the last scattering surface observed by Planck.

the fiducial value $\epsilon_{\rm a}=\epsilon_{\rm a,0}$, and up to $f_{\rm *,m}\lesssim 2\times 10^{-3}$ for $\epsilon_{\rm a}/\epsilon_{\rm a,0}\sim 0.3$ (see Figure 3).

Finally, we demonstrated that the inclusion of DSs can suppress the optical depth further than LW feedback alone, making it possible that the integrated optical depth is consistent with the Planck data, and can also do so in the absence of LW feedback so long as $f_{\rm DS}$ is large enough (see Figure 5). While LW feedback by itself can maximally decrease the integrated optical depth down to $\tau \sim 0.05$ as discussed above, DSs can easily attain $\tau < 0.05$ for a larger range of astrophysical parameters. We note that while the small values of $f_{*,\rm m}$ required by LW feedback are still consistent

with hydrodynamical cosmological simulations (Skinner & Wise 2020), DSs can accommodate larger/more moderate values of the star formation efficiency, which may become increasingly interesting with future simulations.

The possibility of probing DSs presents opportunities to gain valuable insight about star formation and the nature of nonbaryonic DM. As we demonstrate here, these fascinating objects can address the small value of the integrated optical depth to the last scattering surface, which makes them interesting targets to pursue. Furthermore, since the optical depth, as a single number, does not uniquely determine the ionization history,

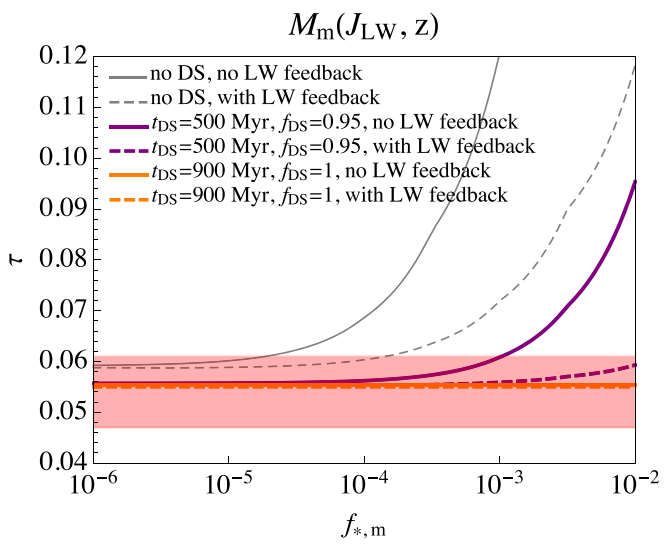


Figure 5. The integrated optical depth to the last scattering surface as a function of minihalo star formation efficiency, $f_{*,\rm m}$, when $\epsilon_{\rm a}=\epsilon_{\rm a,0}$, and $M_{\rm m}=M_{\rm m}/J_{\rm LW}$, z). Gray solid (dashed) curve corresponds to a reionization history without DSs and in the absence (presence) of LW feedback, purple solid (dashed) curve represents reionization in the presence of DSs with $t_{\rm DS}=500~{\rm Myr}$, $f_{\rm DS}=0.95~{\rm without}$ (with) LW feedback, and orange solid (dashed) curve shows the effect of DSs with $t_{\rm DS}=900~{\rm Myr}$, $f_{\rm DS}=1~{\rm on}$ reionization history, without (with) LW feedback. The red band displays the 1σ region based on the integrated optical depth to the last scattering surface observed by Planck.

additional cosmological observables such as the ground-state hyperfine transition, corresponding to wavelength of 21 cm (Furlanetto et al. 2006; Pritchard & Loeb 2012), can provide a more detailed picture of the role of DSs in the reionization process. There are a variety of ways to search for indirect signals of DS remnants today (Rindler-Daller et al. 2015, 2021). For DS that survived to lower redshifts, it is even possible that they will be directly observed by the James Webb Space Telescope (Freese et al. 2010; Zackrisson et al. 2010; Ilie et al. 2012).

The work of P.G., P.S., and B.S. is supported in part by NSF grant PHY-2014075. The work of E.V. is supported in part by NSF grant AST-2009309 and NASA grant 80NSSC22K0629. P.G. is very grateful to Prof. Masahide Yamaguchi for his generous support under JSPS Grant-in-Aid for Scientific Research No. JP18K18764 at the Tokyo Institute of Technology. P.S. would like to thank Katherine Freese and Chris Kelso for useful preliminary discussions.

ORCID iDs

surname>Shams Es Haghi https://orcid.org/0000-0001-9563-0299

Eli Visbal https://orcid.org/0000-0002-8365-0337

References

Abel, T., Bryan, G. L., & Norman, M. L. 2002, Sci, 295, 93 Ahn, K., & Shapiro, P. R. 2021, ApJ, 914, 44

```
Bauer, A., Springel, V., Vogelsberger, M., et al. 2015, MNRAS, 453, 3593
Benson, A. J., Sugiyama, N., Nusser, A., & Lacey, C. G. 2006, MNRAS,
  369, 1055
Bromm, V., Coppi, P. S., & Larson, R. B. 2002, ApJ, 564, 23
Bromm, V., Kudritzki, R. P., & Loeb, A. 2001, ApJ, 552, 464
Ciardi, B., Ferrara, A., Governato, F., & Jenkins, A. 2000, MNRAS, 314, 611
Dawson, S., Rhoads, J. E., Malhotra, S., et al. 2007, ApJ, 671, 1227
Dijkstra, M., Haiman, Z., Rees, M. J., & Weinberg, D. H. 2004, ApJ, 601, 666
Fan, X., Strauss, M. A., Becker, R. H., et al. 2006, AJ, 132, 117
Fernandez, R., Bryan, G. L., Haiman, Z., & Li, M. 2014, MNRAS, 439, 3798
Fialkov, A. 2014, IJMPD, 23, 1430017
Fialkov, A., Barkana, R., Visbal, E., Tseliakhovich, D., & Hirata, C. M. 2013,
   MNRAS, 432, 2909
Freese, K., Bodenheimer, P., Spolyar, D., & Gondolo, P. 2008, ApJL,
  685, L101
Freese, K., Ilie, C., Spolyar, D., Valluri, M., & Bodenheimer, P. 2010, ApJ,
Freese, K., Rindler-Daller, T., Spolyar, D., & Valluri, M. 2016, RPPh, 79,
Furlanetto, S. R., Oh, S. P., & Briggs, F. H. 2006, PhR, 433, 181
Gnedin, N. Y. 2000, ApJ, 542, 53.
Greif, T. H., Bromm, V., Clark, P. C., et al. 2012, in AIP Conf. Proc. 1480,
  First Stars IV-from Hayashi to the Future, ed. M. Umemura & K. Omukai
  (Melville, NY: AIP), 51
Haiman, Z., & Holder, G. P. 2003, ApJ, 595, 1
Haiman, Z., Rees, M. J., & Loeb, A. 1997, ApJ, 476, 458
Haiman, Z., Thoul, A. A., & Loeb, A. 1996, ApJ, 464, 523
Hartwig, T., Magg, M., Chen, L.-H., et al. 2022, arXiv:2206.00223
Ilie, C., Freese, K., Valluri, M., Iliev, I. T., & Shapiro, P. R. 2012, MNRAS,
  422, 2164
Komatsu, E., Smith, K. M., Dunkley, J., et al. 2011, ApJS, 192, 18
Kulkarni, M., Visbal, E., & Bryan, G. L. 2021, ApJ, 917, 40
Leitherer, C., Schaerer, D., Goldader, J. D., et al. 1999, ApJS, 123, 3
Machacek, M. E., Bryan, G. L., & Abel, T. 2001, ApJ, 548, 509
Natarajan, A., Tan, J. C., & O'Shea, B. W. 2009, ApJ, 692, 574
O'Shea, B. W., & Norman, M. L. 2008, ApJ, 673, 14
Planck Collaboration, Ade, P. A. R., Aghanim, N., et al. 2016, A&A, 594, A13
Planck Collaboration, Aghanim, N., Akrami, Y., et al. 2020, A&A, 641, A6
Pritchard, J. R., & Loeb, A. 2012, RPPh, 75, 086901
Rindler-Daller, T., Freese, K., Townsend, R. H. D., & Visinelli, L. 2021,
           , 503, 3677
Rindler-Daller, T., Montgomery, M. H., Freese, K., Winget, D. E., &
  Paxton, B. 2015, ApJ, 799, 210
Samui, S., Srianand, R., & Subramanian, K. 2007, MNRAS, 377, 285
Schaerer, D. 2002, A&A, 382, 28
Schaerer, D. 2003, A&A, 397, 527
Schauer, A. T. P., Glover, S. C. O., Klessen, R. S., & Ceverino, D. 2019,
   MNRAS, 484, 3510
Schleicher, D. R. G., Banerjee, R., & Klessen, R. S. 2009, PhRvD, 79, 043510
Scott, P., Venkatesan, A., Roebber, E., et al. 2011, ApJ, 742, 129
Sheth, R. K., & Tormen, G. 1999, MNRAS, 308, 119
Skinner, D., & Wise, J. H. 2020, MNRAS, 492, 4386
Spolyar, D., Bodenheimer, P., Freese, K., & Gondolo, P. 2009, ApJ, 705, 1031
Spolyar, D., Freese, K., & Gondolo, P. 2008, PhRvL, 100, 051101
Stacy, A., Greif, T. H., & Bromm, V. 2012, MNRAS, 422, 290
Tegmark, M., Silk, J., Rees, M. J., et al. 1997, ApJ, 474, 1
Tseliakhovich, D., & Hirata, C. 2010, PhRvD, 82, 083520
Tumlinson, J., & Shull, J. M. 2000, ApJL, 528, L65
Tumlinson, J., Shull, J. M., & Venkatesan, A. 2003, ApJ, 584, 608
Visbal, E., Haiman, Z., & Bryan, G. L. 2015, MNRAS, 453, 4456
Visbal, E., Haiman, Z., Terrazas, B., Bryan, G. L., & Barkana, R. 2014,
Wise, J. H., & Abel, T. 2007, ApJ, 671, 1559
Wise, J. H., Demchenko, V. G., Halicek, M. T., et al. 2014, MNRAS,
  442, 2560
Wolcott-Green, J., Haiman, Z., & Bryan, G. L. 2011, MNRAS, 418, 838
Wyithe, J. S. B., & Loeb, A. 2003, ApJL, 588, L69
Zackrisson, E., Scott, P., Rydberg, C.-E., et al. 2010, ApJ, 717, 257
```